Int J Mater Form (2017) 10:717–727
DOI 10.1007/s12289-016-1314-7

ORIGINAL RESEARCH

Numerical study of contact conditions in press hardening for tool wear simulation

Liang Deng[1] · Sergej Mozgovoy[2] · Jens Hardell[2] · Braham Prakash[2] · Mats Oldenburg[1]

Received: 25 April 2016 / Accepted: 18 August 2016 / Published online: 14 September 201 6

Abstract In the press hardening industry, industrial and academic efforts are being directed toward predicting tool wear to realize an economical manufacturing process. Tool wear in press hardening is a tribological response to contact conditions such as pressure and sliding motion. However, these contact conditions are difficult to measure in-situ. Furthermore, press hardening involves high temperatures, and this increases the complexity of the tribo system. The present work investigated the contact conditions of press hardening with a commercial FE code (LS-DYNA) as a base for tool wear simulation. A press hardening experiment was established in industrial environments and evaluated through FE simulations. The numerical model was set up so as to approximate the manufacturing conditions as closely as possible, and the sensitivity with respect to the friction coefficients was examined. The influence of numerical factors such as the penalty value and mesh size on the contact conditions is discussed. The implementation of a modified Archard's wear model in the FE simulation proved the possibility of tool wear simulation in press hardening. Finally, a comparison between the tool wear simulation and the measured wear depth is presented.

Keywords Contact conditions · FE simulation · Press hardening · Archard's wear model

✉ Liang Deng
liang.deng@ltu.se

[1] Division of Mechanics of Solid Materials, Luleå University of Technology, 971 87 Luleå, Sweden

[2] Division of Machine Elements, Luleå University of Technology, 971 87 Luleå, Sweden

Introduction

In order to improve vehicle safety and reduce carbon emission, press hardening is increasingly being used to produce light sheet metal parts with high strength. In the press hardening process, a sheet metal is heated up in a furnace and kept at 930 °C until a fully homogenous austenite phase content is reached. The blank is then transferred to the die position and sequentially formed and quenched in the closed tool until a martensitic state is obtained [11]. The commonly used sheet metal material in the press hardening is 22MnB5 steel, which produces a fully martensitic microstructure after press hardening when quenched in cooled tools. The press hardening process takes advantage of excellent formability of steels at elevated temperature and causes small springback and a remarkable high strength-to-weight ratio to the finished parts. However, the hot forming process requires stamping tools that can endure cyclic loadings and dramatic temperature changes. The relative motion between the austenitised metal sheet and the press hardening tools leads to wear during the forming process. van der Heide and Schipper [9] stated that sliding wear is the dominant wear process in the forming process, in which abrasive wear, adhesive wear, thermal fatigue, and corrosive wear play a role during the entire service life of the tools. Furthermore, oxidation and reactions between the oxide layers as well as the coatings on the blanks and tools increase the complexity of the wear mechanisms. Wear strongly influences not only the performance and quality of the produced parts but also the overall productivity of press hardening in particular and thermomechanical forming in general.

A variety of papers have contributed to the fundamental investigation of the wear in press hardening conditions. The fundamental studies focus on tribological behaviour using laboratory tests mimicking the conditions of the press

hardening process. Hardell and Prakash [8] studied the friction and wear behaviours between boron steels and tool steels from 40 °C to 800 °C through a reciprocating test. In this study, the tribological tests were conducted with plasma nitrided and untreated tool steel pins sliding repeatedly on Al-Si coated boron steel discs at elevated temperatures. The results have shown that friction decreased with increasing temperature whereas wear of the tool steel increased with temperature. Al-Si coated steel shows a significantly low wear rate at 800 °C due to morphological changes. Mozgovoy et al. [15] have studied the tribological behaviour of an uncoated contact pair through reciprocating tests with more test temperatures in the range from 40 °C to 800 °C. The results have shown that the formation of compacted wear debris layers on the surfaces was a main reason when the friction and the wear rate decreased at high temperatures. Hernandez et al. [10] has studied the wear mechanisms at elevated temperatures with a High Temperature Continuous Abrasion Tester. Microploughing and microfatigue were the main wear mechanisms of the used tool steel and the wear rate kept relatively stable from room temperature to 400 °C. At 500 °C and 600 °C, as the tool steel became softer, the embedded wear particles increased and penetrated deeper on the tool surface. Furthermore, some of the wear particles were fractured due to the shearing force at the outermost surface and then further cut the tool surface, which increased the wear rate. At temperatures above 600 °C, the tribolayer consisting of iron oxide and small wear particles was found but it did not reduce the wear rate because the thickness of this layer was negligible compared to the thickness of the plastically deformed layer caused by abrasive particles. Engineers need approaches for predicting tool wear that provides the possibility of extending the tool service life through adjustment of the operating conditions. A contact-mechanics-based wear equation, also called Archard's wear model, was described by Archard and Hirst [1], and it is widely used for metal forming processes. This model postulates that the real contact area is determined by the plastic deformation of contacting asperities and that wear particles are generated owing to the removal of surface asperities under conditions such as load and sliding distance. To implement wear prediction in certain manufacturing processes, researchers modified Archard's wear model because the wear coefficient in this model represents the probability of wear particle generation. Enblom and Berg [3] defined a specific value of the wear coefficient when working in a narrow range of pressure and sliding velocity. Shen et al. [21] employed a combined approach with the finite element (FE) method and Archard's wear model to simulate the progressive wear of contacting surfaces. The authors measured the wear rates by performing pin-on-disc experiments and implemented the removal of material by moving boundary nodes to predict the wear developing in a spherical plain bearing. In a study of wear under high temperature, Stupkiewicz and Mróz [22] found that the interactions occurring in the contact between the tool and the workpiece in a hot forging process caused oxide scaling owing to the hard particles adhering to the workpiece surface. The initial oxide particle concentration had a large influence on the resulting distribution of abrasive wear in the tools. A third body abrasive wear model was developed by generalising Archard's wear model by substituting the normal pressure with the friction stress. To optimize the process parameters, Lee and Jou [13] combined FE simulations with a modified version of Archard's wear model to predict tool wear in a warm forging process, in which the wear coefficient and hardness were determined as functions of temperature. It was found that the tool material exhibited thermal softening and that its wear coefficient increased significantly with temperature. Furthermore, Ersoy-Nürnberg et al. [4] developed a wear coefficient that was correlated with the cumulative wear work (frictional dissipation energy) applied in the modified Archard's wear model. This method made it possible to predict the progression of wear damage at any stage of the tool life cycle by determining the wear coefficients as well as their gradients in deep-drawing experiments. These studies indicate that the application of wear prediction generally defines the wear coefficient as the probability of wear particle generation under significant contact conditions, such as temperature, pressure, and friction.

The present study aims to study the contact conditions occurring on the stamping tool and to explore the possibility of using the FE method in conjunction with Archard's wear model to predict the tool wear in press hardening. To accomplish these objectives, a specific press hardening experiment was established in an industrial environment and evaluated through FE simulations. The present press hardening experiment setup is designed to accelerate the wear process, which decreases the required number of strokes to obtain the measurable wear results. The wear results were used to validate the wear simulation. A user subroutine integrated in a commercial FE code (LS-DYNA) provides the contact conditions used in the tool wear calculation. In addition to deterministic simulations, the present study considers the sensitivity of the contact conditions due to friction coefficients and numerical factors, such as the penalty value and mesh size. A modified Archard's wear model based on the input from a standardised tribological test was implemented for tool wear simulation. The comparison between the tool wear prediction and the measurement was presented based on the tool shape change in the press hardening experiment as measured by a coordinate measurement machine (CMM).

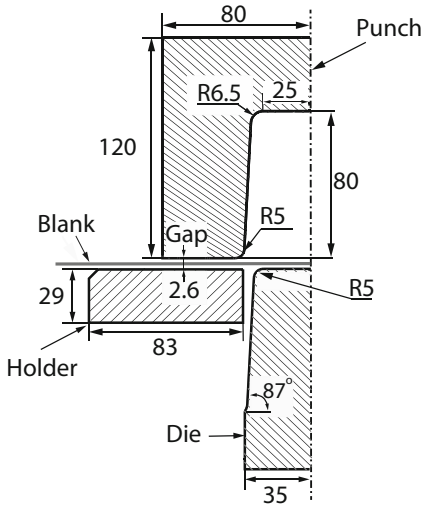

Fig. 1 Illustration of the press hardening experiment (half geometry, left part); all dimensions are in millimetres

Press hardening experiments and simulation

Press hardening experiment

Figure 1 shows the setup of the designed press hardening experiment in one half due to symmetry, which was a part of a production line tool section. The constant gap between the punch and the holder provided frictional sliding of the blank rubbing the tool and increased the contact pressure, which results in an accelerated wear process. Uncoated blanks are used in this investigation and they are frequently used in the industrial process. The aim of this initial study is to model and evaluate basic wear conditions and the more complex behaviour of the Al-Si coating is not included. The process parameters applied in the press hardening experiment are within the ranges of process parameters used in the industrial process. A boron-alloyed steel blank was homogeneously heated to 930 °C in furnace for 5 minutes. The transfer process for the blank to move from the exit of the furnace to the entrance of the die took 9 s. According to a temperature simulation using an effective heat transfer coefficient of 120 $Wm^{-2}K^{-1}$, the temperature in the blank after transfer decreased to 764 °C. The movable punch (upper tool) formed the blank into a target shape with a maximum force of 95 kN while the die (lower tool) kept stationary. With a constant velocity of 100 mms^{-1}, the upper tool was stroked down for 80 mm. To intensify the wear process, the holders accompanied the moving-down punch. When the gap distance between the holders and the punch was set as 2.6 mm, 3.6 mm and 4.6 mm in the FE-simulation of the press hardening experiment, decreasing trends of the contact conditions were obtained in terms of the contact pressure and sliding distance. Since the tool wear is related to the contact conditions assumed by Archard wear model, a small gap distance can accelerate the wear process. Furthermore, the blank thinning was reversely proportional to the gap distances, a smaller gap distance would result in a high risk of cracks of the blank during the forming process. The gap distance of 2.6 mm was chosen to accelerate the wear without the risk of blank cracking. In the forming process, the gap distance of 2.6 mm was maintained, followed by cooling for 11 s. These processes were continuously run 200 times. The number of the strokes was determined by two considerations. Firstly, the number of strokes results in the measurable wear result obtained by the current measuring method mentioned in Section "Wear simulation and validation". Secondly, the quality of the production parts has been degraded. A deep groove of the worn blank produced after 192 strokes is presented in Section "Wear simulation and validation". The material used for the blank was uncoated manganese–boron steel (22MnB5) with a thickness of 1.6 mm, and the stamping tools were made of hot working tool steel (Toolox 44), see Table 1.

Press hardening simulation

In the present study, a numerical model was used to investigate the contact conditions occurring on the stamping tools and to implement the modified Archard's wear model. The established FE simulation based on real manufacturing conditions can be considered as a typical part of a production line. Owing to the symmetry, only half of the press hardening tools were modelled, as shown in Fig. 1. This numerical model includes a blank with dimension of 14 × 132 × 1.6 mm (width × length × thickness) in 3D; however, the blank motion in the width direction was restricted. For the tools, solid elements of 1-mm size were used near the contact surface and larger elements, in the bulk. The blank was modelled using four-node Belyschko–Tsay shell elements with five integration points through the thickness. The initial

Table 1 Alloying compositions (wt%) and initial hardness; Fe makes up the balance

Material	C	Si	Mn	P	S	Cr	Mo	V	Ni	B	$HV_{0.5}$
22MnB5	0.20 – 0.25	0.20 – 0.35	1.0 – 1.3	Max. 0.03	Max. 0.01	0.14 – 0.26	...	...	...	0.005	201 ± 3
Tool steel	0.32	0.6 – 1.1	0.8	Max. 0.001	Max. 0.003	1.35	0.8	0.14	Max. 1	...	458 ± 6

temperature of the blank was above the austenitisation temperature, following which it was decreased to 764 °C before the forming simulation started. An austenite decomposition model predicting austenite decomposition into ferrite, perlite, bainite, and martensite for thin-sheet boron steels has been developed by Åkerström [18]. Consequently, the influence of phase changes on both the mechanical and the thermal properties of the continuously formed and cooled blank was considered in the constitutive model developed by Åkerström et al. [20], which described the phase transformation behaviour of manganese–boron steel. This constitutive model and set of material data applied in a similar crash forming process have been validated by Åkerström and Oldenburg [19]. The forming force measured in the upper tool was in agreement with the calculated force. The tool temperature history measured by thermocouple fixed under the tool surface was consistent to the calculated result. Furthermore, the differences between the calculated and the measured hardness and thickness along each cross section of the formed blank were less than 10 % and 5 % respectively. The positions of the maximum and minimum thicknesses of the formed blank were precisely predicted by the FE simulation. In the present model holder and the upper and lower tools were considered rigid parts, and their initial temperature was set at 40 °C. A constant heat transfer coefficient of 6000 $Wm^{-2}K^{-1}$ was used for the uncoated tool–blank interface. The specific heat capacity C_p and thermal conductivity k of the tool steel were assumed to be the same as those for X40CrMoV5-1 tool material (see Table 2). The static and dynamic friction coefficients for the forming of the uncoated blank were both assumed to be 0.56. This friction value was obtained by a high-temperature tribometer test using uncoated contact pairs, where the boron steel strip was pre-heated until a complete austenite phase and the tool steel pins were kept separated before the sliding process. The test pressures and velocities were within the reasonable ranges in agreement with the present press hardening experiment. A stable friction coefficient of 0.56 was obtained independently of the test velocities and this friction coefficient was regarded as a constant friction coefficient applied in the present press hardening simulation. The detailed setup of the high-temperature tribometer test can be found in work done by Mozgovoy [14].

Table 2 Tool thermal parameters for X40CrMoV5-1 tool material [2]

T (°C)	C_p (J/kg K)	k (W/m K)
20	460	24.6
400	460	26.2
800	460	27.6

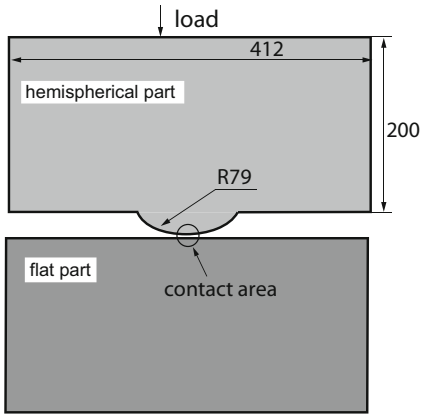

Fig. 2 Dimensions of a spherical contact model; all dimensions are in millimetres

Influence of numerical factors

Because the present contact calculation is based on the penalty method, the inevitable penetration scaling the normal interface force f_n affects the stability of the contact conditions, as seen in the simplified Eq. 1 deduced from Hallquist [7].

$$f_n = \alpha K d \tag{1}$$

where

$$K = \frac{EA}{max(shell\ diagonal)} \tag{2}$$

where α is the scaling factor, K is the stiffness modulus, E is Young's modulus, A is the element area, and d is the penetration depth. Normally, the element sizes used for the tool and the blank are not same because the geometric character of the tool, e.g. the radius needs small elements for a good geometric representation but big elements are used for the rest part of the tool to save computational cost. According to Eq. 2, a large stiffness modulus owing to the big element size causes a large interface force or even a fake bounce. Small elements result in small stiffness modulus. The understanding of the interaction between the mesh size and the stiffness modulus is important for the FE-simulation and a proper scaling factor for the contact calculation determines

Table 3 Test parameters and analytical maximum pressure for spherical contact model

Load (N)	40
Hertzian P_{max} (MPa)	400
Element size of flat part (mm)	1
Element size of hemisphere (mm)	2, 1.4, 1, 0.5, 0.2

Table 4 Calibrated results in spherical contact model

Element size in hemispherical part (mm)	2	1.4	1	0.5	0.2
Penalty scaling factor	0.67	0.80	1.00	0.87	0.27

the accuracy of the present contact-mechanics-based wear simulation.

A 2D spherical contact model was established as shown in Fig. 2, a hemispherical part defined as an elastic body was loaded by a rigid flat part. In order to be consistent to the FE-simulation of press hardening, the spherical contact model was simulated with the explicit solver. The load applied on the bottom of the elastic part was gradually increased. The element size of the flat part was consistent with the element size of the stamping tool. The elastic body mimicking the blank in press hardening was tested with element sizes of 0.2–2 mm; however, the mesh alignment in the contact area was carefully kept. The Hertz contact theory was used for calculating the maximum contact pressure in the elastic body as an analytical solution to compare with the maximum pressure obtained with different numerical factors. Table 3 shows the test parameters and the analytical maximum pressure, where Young's modulus of the flat part was infinitely large because it was defined as a rigid part in the spherical contact model.

Table 4 shows the calibrated penalty scaling values with different element sizes in the hemispherical part. As a simplification, the calibrated penalty scaling factor of the case with 1-mm element size was scaled to 1 as a reference for others. Because the present FE code used the stiffness modulus of the minimum element between the contact parts, bigger element sizes defined in the hemispherical part compared to the element size used in the flat part did not increase the stiffness modulus but resulted in bigger time steps. A big time step led to deeper penetration due to the relation between element size and the stiffness modulus, e.g Eq. 2. In Fig. 4a the cases using the element size of 2 mm and 1.4 mm had very high penetration depths. It was noted that the calibrated penalty factors decreased in the cases using 1 mm to 0.2 mm. In the case with small elements, the contact force is distributed over several nodes, thus the penetration will be smaller, see Fig. 3. On the other hand, smaller elements did not provide the most stable results in terms of less penetration depth and less spurious oscillation. In Fig. 4, the smallest elements of 0.2-mm size led to the apparent waves of penetration depth compared to the other element sizes. Figure 4b shows the gradients of the maximum pressure when the penalty scaling factor was increased slightly from the calibrated values. A higher gradient of the increasing pressure indicated a more unstable contact state in which a small numerical variation can drastically affect the pressure. The bigger element sizes used in the hemispherical part caused higher gradients compared to the case using 1-mm element size for the both parts. The case using the 0.5-mm element size resulted in a very high pressure gradient.

The mesh size of 1 mm with the calibrated penalty factor was the most stable choice, and therefore, it was employed for the blank in the FE simulation of the press hardening experiment.

Contact conditions occurring on stamping tool

In the present press hardening experiment, the tool experienced different blank deformation in different zones as shown in Fig. 5. In the zone 1 and 3, the blank was stretched and bent around the tool radii. In the zone 2, the blank underwent a tensile straining process because the gap between the holder and the punch provided the friction force sticking the blank. Since the upper tool formed the flat blank into the target shape, the upper tool radius (zone 3) experienced the most plastic deformation of the blank and the slight contact occurring on the tool lateral surfaces.

In order to validate the FE-simulation, the blank thickness was measured after the second stroke of the press hardening experiment. A micrometer screw gauge was used to measure specific positions along the center section in the formed blank, as seen in Fig. 6. Each position spacing by 10 mm was measured by 20 times and the average value was compare to the calculated thickness of the forming simulation. Figure 6b presents a thickness comparison,

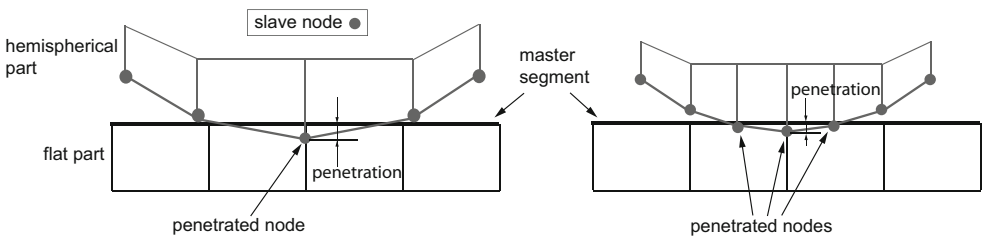

Fig. 3 Illustration of the penetrated nodes when small elements and big elements are used in hemispherical part

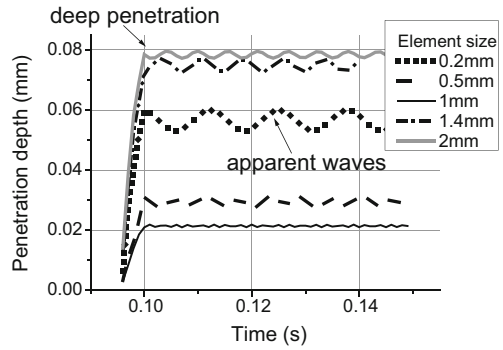

(a) Penetration depths

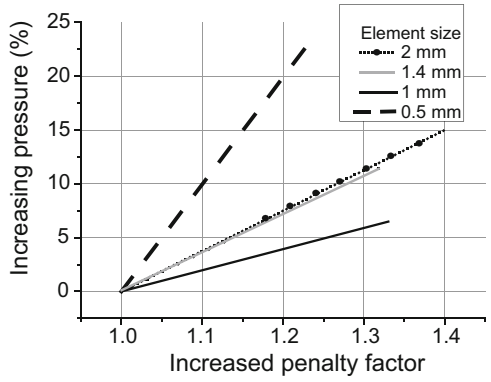

(b) Variational maximum pressure

Fig. 4 Influence on the penetration (**a**) and the maximum pressure (**b**) by the penalty scaling factor and element size

where the predicted thickness variations along the specific positions were consistent to the tendency of the measured thickness. The difference in most positions may attribute to the tolerance of the initial blank thickness. The thickness difference between the measured and calculated values in position 7 can be explained in terms of the thinning of the blank caused by actually higher friction between the holder and the punch compared to the friction coefficient used in the FE-simulation.

A user subroutine integrated with LS-DYNA was used to extract the contact conditions in terms of the sliding

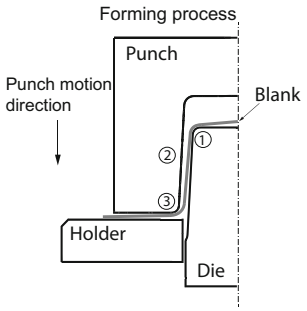

Fig. 5 Forming process of the press hardening model with different zones: zone 1 is the die radius, zone 2 refers to the both tool lateral surfaces, zone 3 is the punch radius

distance, sliding velocity, contact temperature, and contact pressure from the contacting nodes during the drawing process. In each explicit time step, the FE code calculated the relative motion between the blank and the tool, the summation of which gave the sliding distance; dividing this distance by the time step gave the relative velocity. The contact information was output at 0.01-s intervals. The nodal pressure was the quotient of the normal force and the fraction area of the elements connecting to the node. Table 5 shows a statistical overview of the contact conditions evaluated on the upper tool from the press hardening simulation, where the element size of the blank was 1 mm. It should be noted that the mean values of the transient values such as contact pressure and sliding velocities were the averages of the contact conditions occurring on all contacting nodes in the entire drawing process, whereas the statistical data of sliding distance was calculated by the final and accumulated values. The high standard deviations of the surface temperature, contact pressure, sliding distance and sliding velocity represent the contact conditions that were unevenly distributed in the contact area and the harsh conditions concentrated on the upper tool radius when the blank was bent around the tool radius.

According to the radius direction shown in Fig. 7, the contact pressures and tool temperatures measured from different sub-sections in the upper tool radius and averaged over the blank width are shown in Fig. 8. The small pressure peaks in sub-sections 3 and 4 at around 0.2 s were due to the impact effect when the upper radius initially touched the blank. The frequency oscillation was attributed to the different stiffness modulus between segments, which was amplified when the blank slid along the radius. Subsections 3, 4 and 5 from 26°–51° of the radius were critical areas and experienced high pressures. The front part, subsection 1, only experienced short-duration contact at the beginning of the drawing process; the contact between the end part of the punch radius and the blank occurred when the tools closed, as indicated by the pressure curve measured in sub-section 7. A similar observation was made for the tool temperature; the temperature evaluated in sub-section 3 increased drastically at the beginning of drawing while the end part of the radius was heated later, as indicated by the temperature curve of sub–section 7. The rising tool temperature observed implied that stagnation between the tool and the pass-by blank caused increased heat transfer.

An extended range of constant friction coefficients was applied in the present model in order to study the influence of the friction on the contact conditions. The selected range of friction coefficient has been reported in literature from different tests with uncoated and Al-Si coated blanks, see Karbasian and Tekkaya [11] and Naganathan and Penter [16]. The resulting contact conditions are presented in Table 6. The variation percent in the contact condition

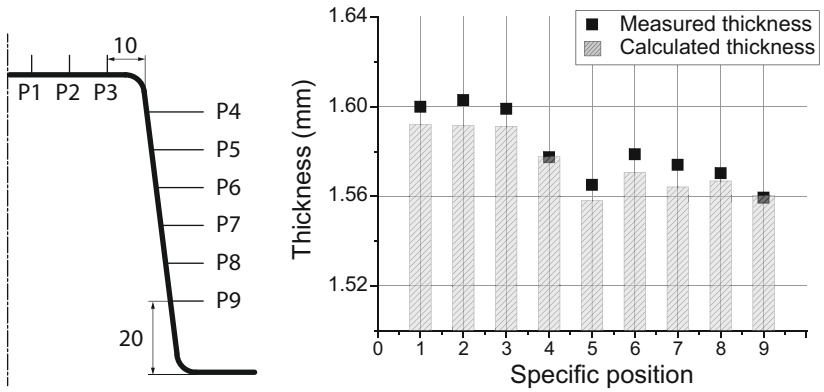

(a) Specific positions on the formed blank, all dimensions are in millimetres

(b) Thickness comparison

Fig. 6 Validation of FE-simulation through blank thickness comparison

referring to the ratio between difference and average illustrates the influence of the extended friction coefficients on the contact conditions as seen in Fig. 9. The higher friction coefficient defined in the numerical model provided a stronger sticking effect between the blank and the tool, and higher pressure and sliding distance were observed. The variation in friction coefficients dramatically affected the maximum pressure in the tool, which variation percent reached 48.2 %. Furthermore, more friction energy due to the higher friction coefficient led to higher tool temperature and the variation reached 24.3 %. The variation in friction range did not significantly influence the maximum sliding distance.

Wear simulation and validation

In the present study, a standardised tribological experiment, the pin-on-disc test, performed by Mozgovoy et al. [15] with uncoated samples was used to provide the input to Archard's wear model. In the pin-on-disc test, the generated wear particles were repeatedly compressed during the reciprocating sliding process and the formation of the protective wear debris layers prevented the further wear. The repeated sliding process gives a similar effect as the protective wear debris layers in the worn stamping tool. The worn stamping tool needs to be reground when it has been experienced around 3000 strokes as mentioned by Pelcastre et al. [17]. The wear coefficient in Archard's wear model was treated as a function of temperature through a regression analysis of the experimental results. The present wear prediction employed the experimental results at 40 °C, 200 °C and 400 °C that covered the maximum tool temperature obtained from the FE simulation of the press hardening experiment. Two reasons were considered in the choice of the nominal pressure of 10 MPa in the pin-on-disc test. Firstly, the real contact area, generally, was much smaller than the nominal area of the pin. Secondly, the pin entraps in the hot, and soft disc if a very high load used in the pin-on-disc test. To predict wear through a numerical model of stamping, the weight loss obtained in the pin-on-disc test was converted into the wear depth value used in the wear calculation. However, the present wear simulation neglected complex wear mechanisms such as abrasion and adhesion combined with oxidation. The wear coefficient in consideration of the overlapping of several mechanical and thermal phenomena was used to predict the volume loss. Owing to the variation of pressure during the drawing process, the integral of the sliding velocity v over the time step dt was used to replace the sliding distance L. Then, the modified Archard's wear

Table 5 Contact conditions occurring on the upper tool in press hardening simulation

Upper tool				
Parameter	Contact pressure (MPa)	Surface temperature (°C)	Sliding distance (m)	Sliding velocity (m/s)
Maximum	94.5	302	0.0612	0.183
Mean	18.924	177.162	0.00372	0.0719
Standard deviation	18.649	69.452	0.0115	0.0374

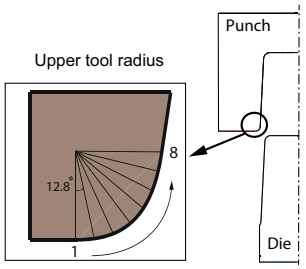

Fig. 7 Illustration of direction and sub-sections of punch (upper tool) radius

model relating to the thickness of the material removed by wear with the pressure, the sliding distance and the hardness of the blank is defined:

$$W(T) = K(T)\frac{PL}{H(T)} \tag{3}$$

where $W(T)$ is the temperature-dependent wear depth; $K(T)$, the wear coefficient, P, the pressure; and $H(T)$, the temperature-dependent hardness of the 22MnB5 steel as measured by Hernandez et al. [10] through a specially developed hot hardness tester.

Gupta [6] developed a generalised wear model that accounted for mechanical as well as several thermally activated processes leading to wear; the temperature-dependent

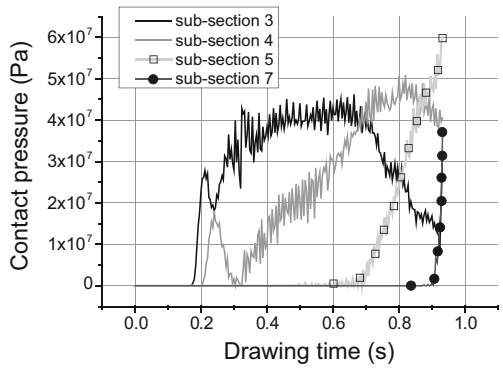

(a) Contact pressure

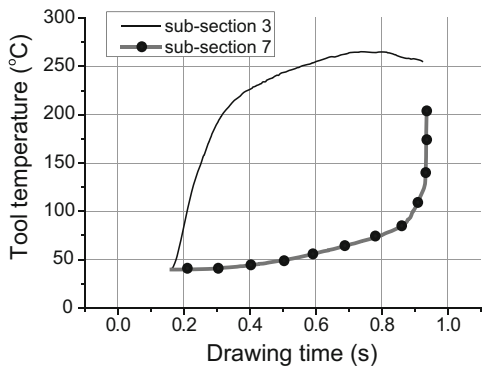

(b) Surface temperature

Fig. 8 Contact conditions occurring on upper tool radius

Table 6 Contact conditions occurring on the upper tool due to variational friction coefficients

Friction coefficient	0.2	0.4	0.7
Maximum pressure (MPa)	71.5	87.5	116.0
Maximum sliding distance (m)	0.0569	0.0598	0.0613
Maximum surface temperature (°C)	261	276	332

wear coefficient was derived by fitting the model to actual experimental data. This method introduces a reference temperature at which the total wear reduces to Archard's wear equation. Then, the thermal rate contribution would vanish, and Archard's wear rate could be represented by the wear rate in vacuum at the reference temperature. However, this wear rate is commonly not available, and therefore, a regression model of the following form was used instead for the wear coefficient:

$$K(T) = ae^{bT} + ce^{dT} \tag{4}$$

where a, b, c, and d are unknown parameters of the regression model. The present temperature-dependent wear coefficient was calculated using Eq. 5, and it can be curve fitted using Eq. 4.

$$K(T) = \frac{V(T)\,H(T)}{F\,L} \tag{5}$$

where F is the load applied in standardised tribological experiments and V, the loss volume measured by the weight change of the sample. The parameters of the applied Archard's wear model is summarized in Table 7.

A topological measurement of the worn blank produced after 192 strokes was carried out by a WYKO 3D optical profilometer, as seen in Fig. 10. This measurement was performed with a 2.5× optical objective and a 1× image zoom lens. The measurement scope was 1.9 × 2.5 mm and located in position 6 as shown in Fig. 6a The deep of the groove on the worn blank surface in relation to the reference plane (defined by the surrounding flat surface) was 70 um. Regrinding operation for the tool would be needed in a production line due to such a produced part with the degraded quality. The wear profile of the worn blank surface was in agreement with the groove profile formed in the abrasive

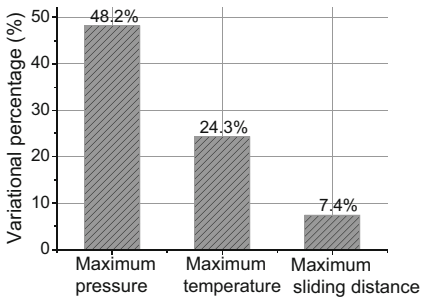

Fig. 9 Variation percent in contact conditions

Table 7 Wear coefficient fitting parameters

Material	Pressure	Fitting parameters				adj. R^2
	(MPa)	a	b	c	d	
Tool steel	10	2.264×10^{-2}	– 0.0120	3.761×10^{-8}	0.0062	0.9630

wear process. Kato and Adachi [12] stated that in the abrasive wear process the grooves are formed as the result of the generated wear particles scratching on the surface and plastic flow of material forms ridges on both sides of a groove. In the present study, the tips of the ridges were compressed and formed into flat shapes when the blank was bent around the tool radius. Two relatively small ridges formed in one side of the grooves was attributed to the abrasive wear of the entrapment of the wear particles in the interface between the ridge and the tool.

Additionally, the scratching track formed on the worn blank surface implied a hard adhesion built up in the counter surface.

A ZESIS Contura G2 coordinate measuring machine (CMM) was used to measure the shape changes of the upper tool radius after 200 continuous strokes because the measurable wear concentrated to the upper tool radius and this observation was consistent to the wear simulation. The probe measured seven positions distributed evenly along the radius for 90 °. The first measurement was performed on the original tool and the second one, at the same positions after 200 strokes of press hardening. The different distances from the measured coordinates to the radius centre were considered shape changes due to wear. The nominal machine accuracy is 1 μm; however, the real maximum error can reach 6 μm. Because the original measurement was performed before the press hardening experiment, the severest wear scar may not be present at the measured positions. This deviation between the severest wear scar and the measured positions affects the validation of tool wear prediction. To ensure accuracy, the CMM measurements were performed by four times at different width positions on the upper tool radius.

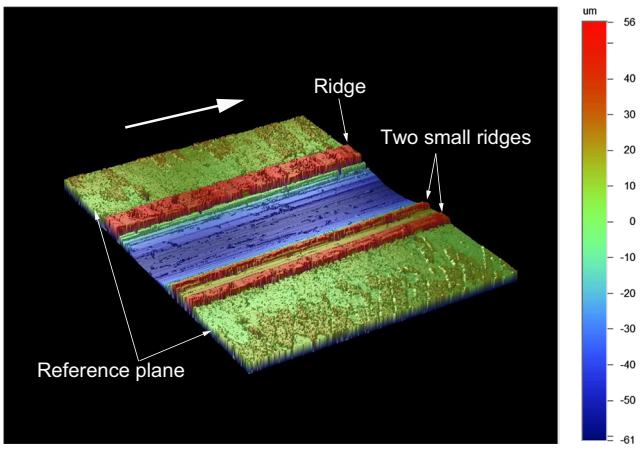

Fig. 10 3D surface profile of the worn blank after 192 strokes, the big arrow indicates the direction of the relative motion of blank

Based on the tool wear simulation using LS-DYNA, the statistical analysis of the wear depths of the upper tool in which the wear depth was linearly extrapolated by 200 times after one drawing simulation is shown in Table 8. The mean value and standard deviation indicate that wear was distributed unevenly. The extended range of the friction coefficient, cf. Table 6, resulted in the maximum wear depth range of 7.3 %. Figure 11 (a) shows the predicted concentration of wear on the upper tool radius, which was the part that experienced the most contact behaviour. Additionally, the blank with 2-mm mesh size with a calibrated penalty factor led to smaller maximum wear depth of 0.0103 mm owing to the smaller sliding distance predicted. The wear depths at the sub-sections were averaged from the nodes distributed along the blank width, the variation of which was attributed to the thickness changing of the blank during the drawing process. Figure 11b shows the wear profiles of the prediction and the measurement on the punch radius and the reference line referring to zero shape deviation indicates the initial tool shape.

The negative shape deviation can be regarded as wear depth and the positive shape deviation was the built-up material adhered on the tool surface exceeding the tool shape (indicated by the reference line in Fig. 11b). The position of the highest wear depth at 30 degrees related to the harsh contact conditions, e.g the contact conditions in subsection 3 shown in Fig. 8, was predicted by the present wear simulation. However, since the valleys formed on the tool surface due to wear act as reservoirs for wear debris [17], the area indicated by 1 and 2 were the accumulation

Table 8 Prediction of the extrapolated wear depth for 1-mm blank element size

Wear depth (mm)		
Maximum	Mean	Standard deviation
0.0162	0.000715	0.00217

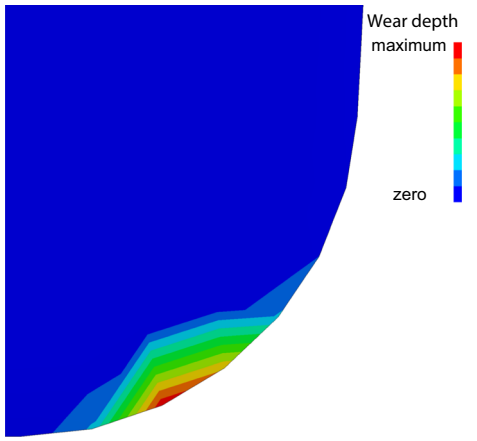

(a) Predicted wear distribution in centre section

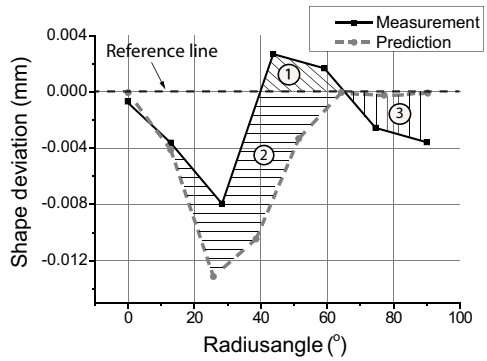

(b) Wear profile

Fig. 11 Wear depth on upper tool radius for 1-mm blank element size

of the wear debris caused by repeated compressions of the increasing pressures in sub-section 4 and 5 (see Fig. 8a) during 200 strokes. The severe contact conditions in sub-section 7 in the end of forming process (see Fig. 8) may cause three-body abrasive wear in the end part of the radius (area 3) due to the break-off of the significant adhesion indicated by area 1. This wear result was consistent to the statement that when the initial adhesion takes place at asperities due to the formation of bonding junctions and increase in size as sliding motion continues, the built-up adhered fragment may break away due to plastic shearing and cause three-body abrasive wear [5]. The discrepancy between the measurement and the prediction implied the limitation that the employed Archard's wear model based on the standardised tribological test used a positive wear coefficient. The present wear coefficient represented the probability of the generation of the wear particles under the experimented condition, and the development of wear particles in the interface in terms of the adhesion and the consequent three-body abrasion due to the break-away of the adhesion was not captured.

Conclusions

This study aimed to investigate the contact conditions causing tool wear in press hardening through FE-simulations and to explore the possibility of the application of tool wear simulation. To calibrate numerical factors such as the mesh size and penalty factor, a spherical contact model was studied. By using the calibrated mesh size and penalty scaling factor, the FE simulation of the press hardening experiment predicted the contact profiles, such as the pressure and tool temperature, occurring on the upper tool radius. The statistical analysis of the contact conditions provided a base to design an experiment that reproduces the tribological behaviour of press hardening. It was noted that increased friction coefficient caused increased pressure and sliding distance in the present FE simulation of the press hardening experiment. A modified Archard's wear model with a temperature-dependent wear coefficient was implemented in the tool wear simulation. The relatively good agreement between the FE simulation using the modified Archard's wear model and the experimental results demonstrated the practical significance of the tool wear simulation. However, the present tool wear simulation is dependent of the choice of numerical factors, the variation in friction and the input data for the employed wear model. Furthermore, the employed wear model predicting the wear particle generation resulted in negative wear depths but the wear measurement of the upper tool radius indicated that the adhesion of wear particles existed. With the contact conditions calculated by the FE simulation of the press hardening experiment, the mechanism behind the adhesion can be explained. The difference in the wear prediction based on the present method and the measurement motivated the researchers to develop a more elaborated laboratory test. Further studies will focus on a redesigned tribological experiment with interrupted sliding processes to obtain a deep understanding of the mechanism behind the adhesion. In order to capture both abrasive and adhesive wear, relevant physical factors need to be introduced into the modelling of wear in press hardening processes.

Acknowledgments This work was funded by the Swedish Governmental Agency for Innovation Systems (Vinnova) programme FFI – Sustainable Production Technology. The authors wish to express their gratitude for this support. The authors gratefully acknowledge SSAB EMEA AB, Oxelösund, Sweden, for providing the tool material and Gestamp HardTech AB, Luleå, Sweden, for performing the press hardening experiment. Finally, the authors would like to thank Ionbond Sweden AB, Oerlikon Balzers Sandvik Coating AB, and Swerea Mefos AB for their keen interest in this study.

Compliance with Ethical Standards

Funding This study was funded by Vinnova (grant number 2010-02851).

Conflict of interests The authors declare that they have no conflict of interest.

References

1. Archard JF, Hirst W (1956) The wear of metals under unlubricated conditions. Proc R Soc London A: Math Phys Eng Sci 236(1206):397–410
2. Bergman G (1999) Modelling and simulation of simultaneous forming and quenching, phd thesis. PhD thesis, Luleå University of Technology, Luleå, Sweden
3. Enblom R, Berg M (2008) Approach procedure and trial simulation of rail profile evolution due to uniform wear. J Rail Rapid Transit 222:15–25
4. Ersoy-Nürnberg K, amd M Golle GN, Hoffmann H (2008) Simulation of wear on sheet metal forming-an energy approach. Wear 265:1801–1807
5. Gahr K (1987) Microstructure and wear of materials, tribology series. Elsevier Science, https://books.google.se/books?id=qibApT7zNcYC
6. Gupta PK (2001) On a multi–process wear model. Lubri Eng 57(4):19–24
7. Hallquist JO (2006) LS–DYNA theory manual. Livemore
8. Hardell J, Prakash B (2008) High-temperature friction and wear behaviour of different tool steels during sliding against al-si-coated high-strength steel. Tribol Int 41(7):663–671
9. van der Heide E, Schipper DJ (2004) Tribology in metal forming. CRC Press, chap 10, pp 347–374
10. Hernandez S, Hardell J, Winkelmann H, Ripoll MR, Prakash B (2015) Influence of temperature on abrasive wear of boron steel and hot forming tool steels. J Wear 338–339:27–35
11. Karbasian H, Tekkaya A (2010) A review on hot stamping. J Mater Process Technol 210(15):2103–2118
12. Kato K, Adachi K (2000) Wear mechanisms. In: Bhushan B (ed) Modern tribology handbook, vol 7. CRC Press, pp 273–300
13. Lee RS, Jou JL (2003) Application of numerical simulation for wear analysis of warm forging die. J Mater Process Technol 140(1–3):43–48
14. Mozgovoy S (2014) High temperature friction and wear in press hardening. Licentiate thesis, Luleå University of Technology, Luleå, Sweden
15. Mozgovoy S, Hardell J, Deng L, Oldenburg M, Prakash B (2014) Effect of temperature on friction and wear of prehardened tool steel during sliding against 22mnb5 steel. Tribol Mater Surf Interf 8(2):65–73
16. Naganathan A, Penter L (2012) Hot stamping. In: Altan T, Tekkaya A (eds) Sheet metal forming-processes and applications, vol 7. ASM International, pp 133–156
17. Pelcastre L, Hardell J, Prakash B (2011) Investigations into the occurrence of galling during hot forming of al-si-coated high-strength steel. Proc Inst Mech Eng Part J: J Eng Tribol 225:487–498
18. Åkerström P (2006) Modelling and simulation of hot stamping. PhD thesis, Luleå University of Technology, Luleå, Sweden
19. Åkerström P, Oldenburg M (2008) Numerical simulation of a thermo-mechanical sheet metal forming experiment. In: Numisheet 2008: Proc. 7th int. conf. and workshop on numerical simulation of 3D sheet metal forming processes. Interlaken, Switzerland, pp 569–574
20. Åkerström P, Bergman G, Oldenburg M (2007) Numerical implementation of a constitutive model for simulation of hot stamping. Modell Simul Mater Sci Eng 15:105. http://stacks.iop.org/0965-0393/15/i=2/a=007
21. Shen X, Cao L, Li R (2010) Numerical simulation of sliding wear based on archard model. In: Mechanic automation and control engineering (MACE). IEEE, Wuhan, pp 325–329
22. Stupkiewicz S, Mróz Z (1999) A model of third body abrasive friction and wear in hot metal forming. Wear 231(1):124–138